Frontiers in Bioscience Landmark

Front. Biosci. (Landmark Ed) **2025**; 30(1): 25565
https://doi.org/10.31083/FBL25565

Original Research

Trimetazidine: Activating AMPK Signal to Ameliorate Coronary Microcirculation Dysfunction after Myocardial Infarction

Xiaolong Qu[1,2], Pan Yang[3], Li Jiao[4], Yuehui Yin[1,*]

[1]Department of Cardiology, The Second Affiliated Hospital of Chongqing Medical University, 401336 Chongqing, China
[2]Department of Cardiovascular Medicine, Southwest Hospital, Army Medical University, 400038 Chongqing, China
[3]Emergency Department, The Second Affiliated Hospital of Chongqing Medical University, 401336 Chongqing, China
[4]Department of High Altitude Physiology and Pathology, College of High Altitude Military Medicine, Army Military Medical University, 400037 Chongqing, China
*Correspondence: yinyh@hospital.cqmu.edu.cn (Yuehui Yin)
Academic Editor: Natascia Tiso
Submitted: 5 July 2024 Revised: 6 September 2024 Accepted: 14 October 2024 Published: 20 January 2025

Abstract

Background: Myocardial ischemia-reperfusion (I/R) injury and coronary microcirculation dysfunction (CMD) are observed in patients with myocardial infarction after vascular recanalization. The antianginal drug trimetazidine has been demonstrated to exert a protective effect in myocardial ischemia-reperfusion injury. **Objectives**: This study aimed to investigate the role of trimetazidine in endothelial cell dysfunction caused by myocardial I/R injury and thus improve coronary microcirculation. **Methods**: The myocardial I/R mouse model was established, and trimetazidine was administered for 7 days before myocardial I/R model establishment. Echocardiography, 2,3,5-triphenyltetrazolium chloride (TTC) staining, hematoxylin-eosin (H&E) staining, and thioflavin S staining were applied to assess myocardial injury and microvascular function. Additionally, the oxygen-glucose deprivation/reperfusion (OGD/R) model was developed in endothelial cells to simulate myocardial I/R injury *in vitro*. Griess reaction method, immunofluorescence, and western blotting (WB) were employed to detect the expressions of nitric oxide (NO), platelet endothelial cell adhesion molecule-1 (CD31) and vascular endothelial (VE)-cadherin, zonula occludens protein 1 (ZO-1), occludin, vascular endothelial growth factor (VEGF) and adenosine monophosphate (AMP)-activated protein kinase (AMPK) signaling-related proteins in endothelial cells and mouse cardiomyocytes. AMPK pathway inhibitor compound C was used for further mechanism validation. **Results**: Our research demonstrated that trimetazidine can alleviate myocardial pathological injury and cardiac function injury during myocardial I/R. Trimetazidine was observed to improve microvascular reflux phenomenon and microvascular function and barrier injury in myocardial I/R and OGD/R models. Additionally, the expressions of AMPK signal-related proteins were found to be inhibited in myocardial I/R and OGD/R models, which were then activated in mice administered trimetazidine. However, the effects of trimetazidine on endothelial cell function and barrier damage were attenuated after co-treatment with compound C and trimetazidine. **Conclusion**: Trimetazidine ameliorated myocardial I/R-induced CMD by activating AMPK signaling.

Keywords: trimetazidine; coronary microcirculation dysfunction; myocardial infarction; AMPK signal

1. Introduction

Myocardial infarction occurs mainly due to the sudden complete blockage of coronary arteries caused by factors such as atherosclerotic plaque rupture and thrombosis, resulting in the interruption of blood flow to the myocardium and subsequent myocardial cell necrosis [1]. Myocardial ischemia is often a precursor to myocardial infarction and reperfusion is a crucial treatment measure after myocardial infarction [2,3]. However, reperfusion may also cause injury, which known as myocardial ischemia/reperfusion (I/R) injury [4]. Coronary microvascular dysfunction (CMD) plays an important role in the entire process. It is not only related to the occurrence and development of myocardial infarction but also significantly impacts myocardial reperfusion [5]. During myocardial infarction, the microcirculation is damaged due to thrombosis, vascular spasm, and endothelial cell injury [6]. After reperfusion, even if the large coronary arteries are reopened, the microcirculation may still have problems such as no reflow or slow flow, which affects the effectiveness of reperfusion therapy and increases the risk of adverse events such as myocardial infarction expansion, arrhythmia, and heart failure [7,8]. CMD is characterized by structural and functional abnormalities of the coronary microvasculature [9]. Coronary microvascular endothelial damage leads to thrombosis and microvascular occlusion, which is one of the key causes of CMD [10,11]. It is therefore crucial to develop effective strategies for improving coronary microvascular endothelial injury in order to improve the treatment of CMD and myocardial I/R injury.

Trimetazidine, an antianginal drug, has been employed in clinical practice for decades. Recently, trimetazidine has been evidenced to exhibit cardioprotective effects by regulating energy metabolism [12]. Furthermore, trimetazidine has been shown to attenuate pyroptosis in my-

ocardial I/R injury by targeting Gasdermin D (GSDMD) [13]. Early trimetazidine treatment with percutaneous coronary intervention for ST-segment elevation myocardial infarction could reduce myocardial infarction size [14]. Chen and colleagues have elucidated that trimetazidine treatment can alleviate cardiac fibrosis and improve left ventricular dysfunction [15]. These findings suggest that trimetazidine plays a protective role in myocardial injury. However, the question of whether trimetazidine can reduce endothelial cell damage during myocardial I/R remains unanswered.

Collectively, this study aimed to figure out whether trimetazidine can maintain the function of coronary endothelial cells and reduce myocardial I/R injury as well as to discuss its regulatory mechanism. It also aimed to provide a theoretical reference for the selection of drugs for the treatment of CMD and the development of clinical application of trimetazidine.

2. Materials and Methods

2.1 Establishment of the Myocardial I/R Mice

Male C57BL/6 mice (10 weeks) obtained from the Experimental Animal Center at Yangzhou University were raised for 1 week in a SPF animal laboratory with controlled environmental conditions (at 21–23 °C, 60%–65% humidity). The mice were grouped into Control, Sham, I/R, I/R+Vehicle (10% DMSO) and I/R+trimetazidine groups, with 9 mice in each group. Mice in I/R group were intraperitoneally injecting with 1% pentobarbital sodium (40 mg/kg) for anesthetization and fixed in the supine position. After connected with ventilator, the left chest of the mouse were exposed. The left anterior descending coronary artery (LAD) was ligated with a 7-0 ophthalmic suture to completely block the blood flow. Myocardial ischemia was diagnosed when mice presented with st segment elevation and high-amplitude T waves on the ECG. After 30 min of occlusion, the ligature was released and reperfusion was implemented for 24 h. Mice in the Sham group were opened thorax and pericardium, but were not subjected to ligation. Mice in I/R+trimetazidine group or I/R+Vehicle group were orally treated with either trimetazidine (20 mg/kg/d, Cat HY-B0968A, MCE, Monmouth Junction, NJ, USA) or vehicle before I/R injury for 7 days. All mice were sacrificed at the end of the experiment by cervical dislocation. All animal experiments were approved by the ethical committee of Zhaofenghua Biotechnology [IACUC-20221009-03].

2.2 Cardiac Function Test

An animal ultrasound imaging system (Vevo 3100, VisualSonics, Canada) was applied to assess left ventricular end-diastolic diameter (LVEDD) and left ventricular end-systolic diameter (LVESD). Left ventricular ejection fraction (EF) as well as left ventricular fractional shortening (FS) was determined by computer algorithms.

2.3 Measurement of Myocardial Infarct Size

2,3,5-triphenyltetrazolium chloride (TTC) staining was applied for the estimation of myocardial infarct size. The frozen hearts were cut transversally into 1-mm slices and then exposed to 1 % TTC (Cat G3005, Servicebio, Wuhan, China) at 37 °C for 10 min. Image Pro Plus software (Version 6.0, Media Cybernetics, Silver Springs, MD, USA) was employed to express infarct volume. For statistical analysis, we calculated the infarct area of the heart at each level and then multiplied the sum of the infarct area of each heart by the thickness (1 mm) to obtain the total infarct volume. The size of the infarct area was calculated as Infarct volume % = (infarct volume / total volume) $\times$ 100%.

2.4 HE&Staining

Heart tissues were fixed with 4% paraformaldehyde (Cat MKCL5723, Sigma, St. Louis, MO, USA) and paraffin-embedded after 24 hours. Then, the tissues were sectioned into 5-µm sections and were deparaffinized and rehydrated. The sections were stained with hematoxylin solution (Cat 170103, shzychem, Shanghai, China) for 10 min, followed by differentiation in 1% ethanol hydrochloride. The sections were then stained in eosin staining solution (Cat 17372-87-1, shzychem) for 2 min. Finally, the sections were dehydrated and sealed with neutral gum, the results were observed under a microscope.

2.5 Detection of Myocardial Reflow

Thioflavin S (Th-S) staining was employed to measure no-reflow areas [16,17]. Two hours after the end of the cardiac function test, mice were restrained and injected with 200 µL of 1% Th-S (Cat 1326-12-1, Sigma) was via the tail vein. After 2 min, the mice were anaesthetised and sacrificed (by cervical dislocation), and the heart tissue was removed and fixed in 4% paraformaldehyde overnight. The heart tissue was cut into sections with a thickness of 1 mm and sequentially placed on the slides. The results were captured by virtue of a stereo microscope at 359 nm (M205 FCA, Leica, Wetzlar, Germany).

2.6 Griess Reaction Method

Nitric oxide (NO) level in tissues or cells was estimated using Griess reagent Kit (Cat ml076941, mlbio, Shanghai, China). Briefly, the heart tissues were homogenized at 4 °C by adding 10-fold volume of RIPA lysate (Cat BL504A, Biosharp, Hefei, China) to the tissue. Tissue samples were then centrifuged at 10,000 *g* for 15 min at 4 °C, and the supernatant was collected for tissue NO detection. A total of 0.1 mL of tissue or cell supernatant was added to 1 mL of Griess solution. After 15 min, the OD value was determined with the application of a microplate reader (VARIOSKAN LUX, Thermo Scientific, Waltham, MA, USA) at 540 nm.

2.7 Cell Culture

Primary mouse heart microvascular endothelial cells (HCMECs) were extracted from the mouse. Briefly, the hearts of mice were collected in a sterile environment after mice were euthanized and stored in cold PBS. The hearts were trimmed to eliminate excess tissue and major blood vessels, then cut into small fragments measuring 1–2 mm^3. These tissue fragments underwent enzymatic digestion with a combination of collagenase and trypsin at 37 °C for 30 minutes while being gently shaken. The digestion process was halted by adding endothelial cell growth medium containing 10% FBS. The resulting cell suspension was passed through a cell strainer (40–70 μm) and the filtered cells were centrifuged at 1500 rpm for 10 minutes. The cell pellet was resuspended in endothelial cell medium (ECM, Cat 1001, Sciencell, Carlsbad, CA, USA) with 10% FBS (Cat 2068801CP, Thermo Fisher, Waltham, MA, USA) and 1% penicillin-streptomycin (Cat C0222, Beyotime, Shanghai, China) for 3 d at 37 °C with 5% CO_2. The isolated endothelial cells were identified by detection of the endothelial cell marker platelet endothelial cell adhesion molecule-1 (CD31). The cells were passaged every two and a half days. All cell lines were validated by short tandem repeats (STR) profiling and tested negative for mycoplasma. Cells were all cultured in a humidified incubator at 37 °C and 5% CO_2.

2.8 OGD/R Model Induction

The HCMECs were incubated without glucose and 1% O_2-94% N_2-5% CO_2conditions for 4 h. Then, normal medium was replaced and the cells were cultivated under normal conditions for 6, 12 or 24 h. Varying concentrations of trimetazidine (20, 40, and 80 μM, Cat HY-B0968A, MCE, Monmouth Junction, NJ, USA) were applied for the pre-treatment of cells for 24 h prior to oxygen-glucose deprivation/reperfusion (OGD/R) stimulation. The Adenosine Monophosphate (AMP)-activated protein kinase (AMPK) inhibitor compound C (1 μM, Cat HY-13418A, MCE, Monmouth Junction, NJ, USA) was employed for the pre-treatment of cells for 48 h prior to OGD/R stimulation.

2.9 Immunofluorescence (IF)

The myocardial tissue sections were deparaffinized and permeabilized using 0.1% Triton x-100 (Cat 1139ML500, BioFROXX, Germany) for 10 min. Then, the sections were blocked with 5% BSA (Cat 4240GR500, BioFROXX, Germany) for 1 h at room temperature. Meanwhile, after different treatment, mouse heart microvascular endothelial cells (HCMECs) were fixed with 4% paraformaldehyde (Cat MKCL5723, Sigma, St. Louis, MO, USA) for 20 min and then treated with 0.1% Triton x-100 (Cat 1139ML500, BioFROXX, Germany) for 20 min. After being washed, cells were blocked in 5% BSA (Cat 4240GR500, BioFROXX, Germany) for 30 min at room temperature. Subsequently, the sections and cells were exposed to primary antibodies specific to CD31 (1:100, Ab24590, Abcam, Cambridge, MA, USA), vascular endothelial (VE)-cadherin (1:100, AF6265, Affinity, Jiangsu, China) and zonula occludens protein 1 (ZO-1) (1:100, Cat AF5145, Affinity, Jiangsu, China) at 4 °C, followed by cultivation with fluorescein isothiocyanate (FITC) (150 μL) conjugated goat anti-rabbit IgG (Cat GB21301, Servicebio, Wuhan, China) at room temperature for 1 h. Hoechst33258 staining (Cat C1017, Beyotime, Shanghai, China) or DAPI staining solution (Cat C1005, Beyotime, Shanghai, China) was employed for the staining of sections. The photographs were imaged with Olympus X73 fluorescence microscope (Tokyo, Japan). The number of positive cells expressing the target protein was analyzed using ImageJ software 1.49 (NIH, Bethesda, MD, USA). The percentage of cells expressing both CD31 and VE-cadherin was calculated as $CD31^+$VE-$cadherin^+$-positive area (%) = (number of cells expressing both CD31 and VE-cadherin/total number of cells) ×100%. ZO-1 expression was analyzed by ZO-1^+-positive area (%) = (number of cells expressing ZO-1/total number of cells) ×100%. The mean fluorescence intensity (MFI) of VE-cadherin and ZO-1 in cells were calculated as MFI = total Fluorescence Intensity in the cell/the total number of pixels in the cell. The average optical density values for FITC staining were calculated by average optical density = the sum of the weighted fluorescence intensities/the total number of pixels within the cell area.

2.10 Western Blot (WB)

The heart tissues and endothelial cells were homogenized RIPA lysates (Cat BL504A, Biosharp, Hefei, China) to obtain total protein. BCA assay kits (Cat P0012, Beyotime, Shanghai, China) were applied for the quantification of protein concentration. 30 μg of protein for was added into 12% SDS-polyacrylamide gels and transferred to PVDF membranes (Cat IPVH00010, Millipore, Billerica, MA, USA). The membranes were sealed with 5% BSA (Cat 4240GR500, BioFROXX, Germany) and subsequently subjected to primary antibodies at 4 °C overnight. Then the membranes were exposure to secondary antibodies (goat anti-rabbit IgG, 1:5000, ab150077, Abcam, Cambridge, MA, USA) for 2 h at RT. The results were visualized using an ECL kit (Cat WBKLS0100, Millipore, Billerica, MA, USA) and analyzed with ImageJ software. The primary antibodies used in this study included endothelial nitric oxide synthase (eNOS) (1:1000, 27120-1-AP, Wuhan, China), phosphorylated eNOS (p-eNOS) (1:1500, AF3247, Affinity, Jiangsu, China), endothelin-1 (ET-1) (1:1000, 12191-1-AP, Proteintech, Wuhan, China), ZO-1 (1:5000, 21773-1-AP, Proteintech, Wuhan, China), Occludin (1:1000, #91131, CST, Danvers, MA, USA), VE-cadherin (1:1000, 27956-1-AP, Proteintech, Wuhan, China), AMPK (1:2000, 10929-2AP, Proteintech, Wuhan, China), phosphorylated

Adenosine Monophosphate (AMP)-activated protein kinase (p-AMPK) (1:1500, AP1002, ABclonal, Wuhan, China), kruppel-like factor 4 (KLF4) (1:1000, ab241666, Abcam, Cambridge, MA, USA), peroxisome proliferator-activated receptor delta (PPARδ) (1:1000, 60193-1-lg, Proteintech, Wuhan, China), CD31 (1:1000, #77699, CST, Danvers, MA,USA), vascular endothelial growth factor (VEGF) (1:1500, AF5131, Affinity, Jiangsu, China), protein kinase B (AKT) (1:3000, 10176-2-AP, Proteintech, Wuhan, China), phosphorylated AKT (p-AKT) (1:2000, 66444-1-lg, Proteintech, Wuhan, China), phosphatidylinositol 3-Kinase (PI3K) (1:5000, 60225-1-lg, Proteintech, Wuhan, China), phosphorylated-PI3K (p-PI3K) (1:1000, AF4372, Affinity, Jiangsu, China) and GAPDH (1:1500, AF7021, Affinity, Jiangsu, China).

2.11 Cell Counting Kit-8 (CCK-8) Assay

The CCK-8 assay (Cat PR645, Dojindo, Kumamoto, Japan) was performed to detect the cell proliferation capacity. Cells that inoculated into 96-well plates were cultivated for 24 h. Following indicated treatment, added 10 mL of CCK-8 solution into each well and incubate for additional 2 h. A microplate reader (VARIOSKAN LUX, Thermo Scientific, Waltham, MA, USA) was applied to determine the OD at 450 nm.

2.12 Flow Cytometry

Apoptosis was assessed using the double staining with Annexin V-FITC Apoptosis Detection Kit (Cat KCD-T2008, KCT Technology Corporation, Shenzhen, China). Following indicated treatment, 400 µL binding buffer was applied to suspend cells, after which were the exposure to Annexin V-FITC (5 µL) for 10 min and propidium iodide (PI, 10 µL) for 15 min in the dark. Cells were subsequently analyzed using flow cytometry (FACSAria™III, BD Biosciences, San Jose, CA, USA).

2.13 Cell Permeability Detection

The *In Vitro* Vascular Permeability Assay (96-well) kit (Cat ECM642, Merck Millipore, Billerica, MA, USA) was employed for cell permeability detection. Briefly, 125 µL ECM medium was added into the upper chamber to wash the chamber, and then the chamber was placed at room temperature for 15 min. Then 100 µL mouse vascular endothelial cells (1×10^6 cells/mL) were injected into the upper chamber of 96-well transwell plates for 12 h, and 250 µL ECM media was placed on the lower chamber and cultured at 37 °C, 5% CO_2 incubator for 72 h. The cells in the upper chamber were then treated and modeled according to groups for 24 h. And 75 µL of the prepared FITC-Dextran working solution was added to the upper chamber, and 250 µL of ECM medium was added to the lower chamber, and the plates were allowed to stand for 20 min at RT and protected from light. Media were removed from the lower chamber and the fluorescence intensity of each sample was measured with excitation wavelength of 485 nm and emission wavelength of 535 nm by a multifunctional plate reader (VARIOSKAN LUX, Thermo Scientific, Waltham, MA, USA).

2.14 Tubule Formation Assays

HCMECs angiogenesis was observed using µ-slide Angiogenesis (Cat 190807/4, ibidi, Martin rader, Germany). The µ-slide Angiogenesis was placed into a sterile petri dish, and 10 µL of Matrigel (Cat 356231, Corning, Corning, NY, USA) on ice was added to the wells of the µ-slide using a sterile syringe. The µ-slide was then placed into an incubator for 30 min to allow the gel to solidify. Subsequently, 50 µL of cell suspension at the density of 2×10^5 cells/mL were added to the Matrigel matrix and the µ-slide with seeded cells was placed back into the incubator and cultured according to the experimental protocol. Cells were cultivated at 37 °C for 8 h. At last, pictures were imaged and analyzed by means of ImageJ software.

2.15 Statistical Analysis

Student's *t*-test was applied while differences among three or more groups were demonstrated with one-way ANOVA followed by Tukey's post hoc test (GraphPad Prism 8, La Jolla, CA, USA)). *p* less than 0.05 was supposed to indicate statistical significance. All data were exhibited in the format of mean $\pm$ SD.

3. Results

3.1 Trimetazidine Alleviates Myocardial Pathological Injury and Cardiac Function Injury during Myocardial I/R

The echocardiography results showed that compared with the Sham group, EF and FS were greatly decreased, and LVESD was significantly increased after I/R modeling, while there were no significant changes in the LVEDD, indicating that modeling was successful. Following trimetazidine treatment, EF and FS were evidently increased (Fig. 1A,B). TTC staining was utilized for the estimation of myocardial ischemic area. The results showed that by contrast with Sham group, the heart of mice had obvious ischemia after I/R modeling, which was then decreased by trimetazidine treatment, with significant difference (Fig. 1C). The observation of the pathological changes in hearts was implemented with hematoxylin-eosin (H&E) staining. It was discovered that the morphology of cardiomyocytes in the Control group and the Sham group was intact, with normal tissue structure. The myocardium of the I/R group was disorganized, infiltration by numerous inflammatory cells, and a considerable number of myocardial cell necrotic changes, accompanied by hyperplasia of fibrous tissue. The pathological changes observed in the I/R+Vehicle and I/R groups were found to be similar. Following the pre-treatment with trimetazidine, the infiltration of inflammatory cells and necrotic cardiomyocytes were markedly reduced (Fig. 1D).

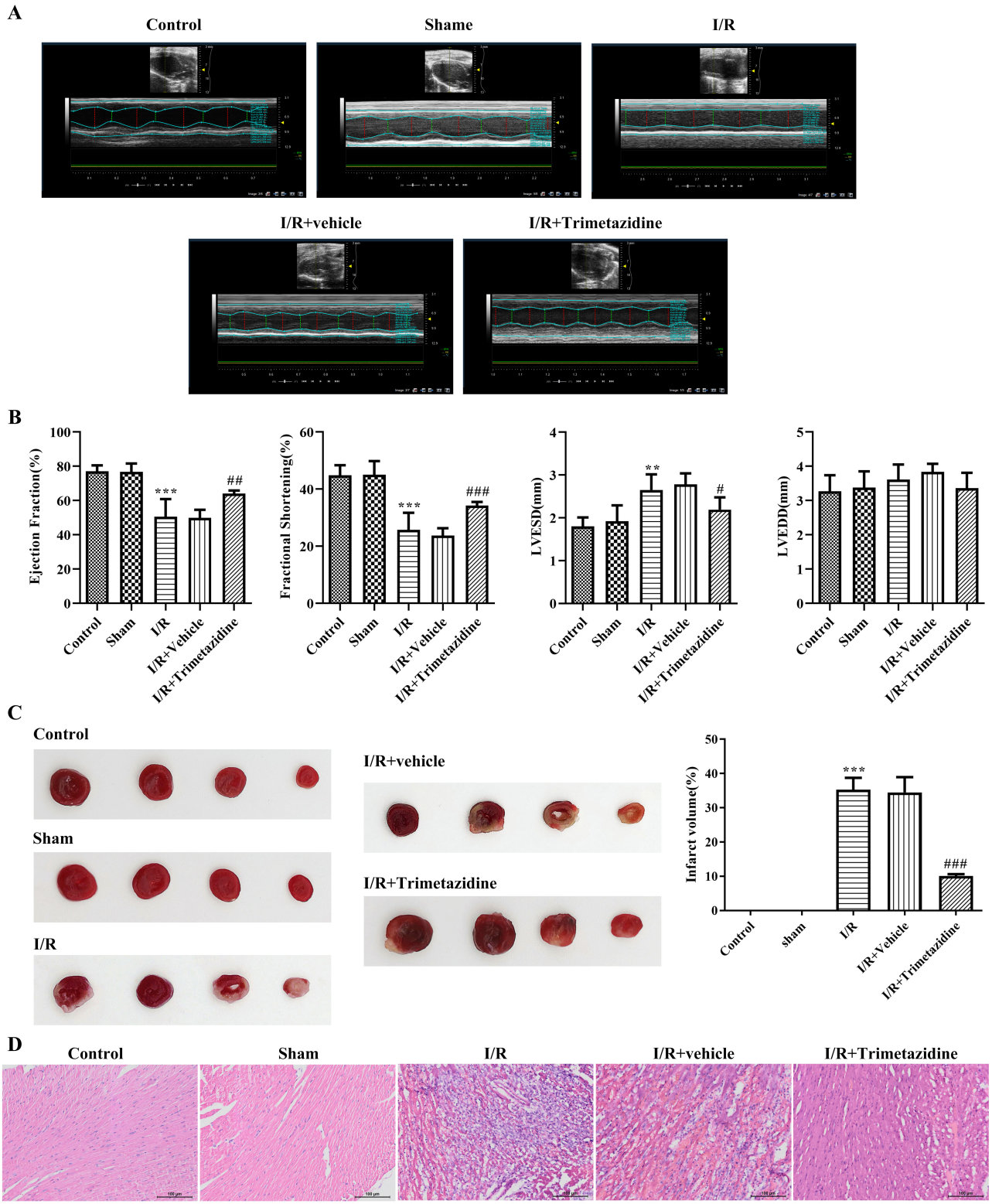

Fig. 1. Trimetazidine alleviates myocardial pathological injury and cardiac function injury during myocardial ischemia/reperfusion (I/R). (A) Cardiac function by echocardiography, n = 6. (B) Quantitative analysis of cardiac function by echocardiography, n = 6. (C) Myocardial ischemic area was detected by 2,3,5-triphenyltetrazolium chloride (TTC) staining, n = 3. (D) H&E staining was used to observe the pathological changes of the heart (scale bar: 100 µm), n = 3. $^{**}p < 0.01$, $^{***}p < 0.001$ vs Sham; $^{\#}p < 0.05$, $^{\#\#}p < 0.01$, $^{\#\#\#}p < 0.001$ vs I/R+Vehicle.

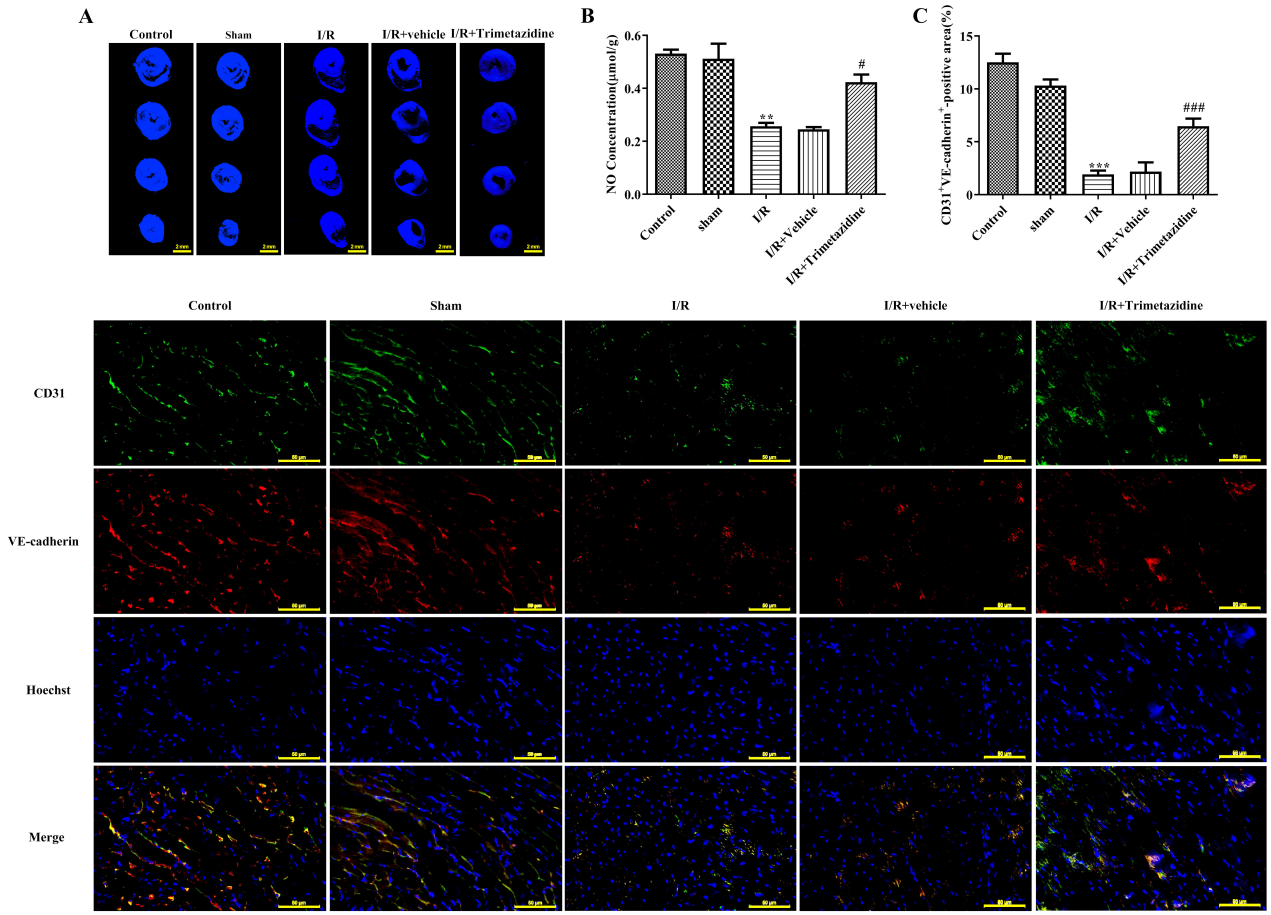

Fig. 2. Trimetazidine improves microvascular reflux, microvascular function and barrier injury during myocardial I/R. (A) Myocardium reflux was measured by thioflavin S (Th-S) staining (scale bar: 2 mm). (B) The nitric oxide (NO) expression in myocardial tissue was detected by Griess reagent Kit. (C) Immunofluorescence (IF) was used to detect platelet endothelial cell adhesion molecule-1 (CD31) and vascular endothelial (VE)-cadherin expression (scale bar: 50 μm). n = 3, $^{**}p < 0.01$, $^{***}p < 0.001$ vs Sham; $^{\#}p < 0.05$, $^{\#\#\#}p < 0.001$ vs I/R+Vehicle.

3.2 Trimetazidine Improves Microvascular Reflux, Microvascular Function and Barrier Injury during Myocardial I/R

Myocardium reflux was evaluated with Th-S staining. The image showed that the bright blue fluorescent area represented the myocardium that had restored blood supply after reperfusion, while some myocardium failed to restore blood flow smoothly and formed no-reflow phenomenon, which is depicted in the figure as a black area. The blood flow was normal in the Control group and Sham group, and there was no distinct diversity between I/R+Vehicle group and I/R group. Trimetazidine pre-treatment can effectively reduce the area without reflux (Fig. 2A). The detection results of NO expression within myocardial tissue exhibited that NO level in myocardial tissue was markedly descended in I/R group, which was subsequently ascended after the intervention with trimetazidine (Fig. 2B). No distinct difference can be found in CD31 and VE-cadherin expression between Control and Sham group. Relative to Sham group, the expressions of CD31 and VE-cadherin in I/R group were remarkably reduced, and there was no distinct difference between I/R+Vehicle group and I/R group. The expressions of CD31 and VE-cadherin were greatly elevated after the pre-treatment with trimetazidine (Fig. 2C).

In addition, trimetazidine increased the expressions of ZO-1 in the heart tissue of mice compared with the I/R+Vehicle group and I/R group (Fig. 3A). Results obtained from WB revealed that by contrast with Control group and Sham group, the expressions of eNOS, p-eNOS, ZO-1, Occludin and VE-cedherin in I/R group were conspicuously decreased, while ET-1 expression was significantly elevated, which were then reversed following the intervention of trimetazidine (Fig. 3B). Moreover, we examined the activation of PI3K/AKT, a signaling pathway upstream of eNOS. The results showed that the ratio of p-PI3K/PI3K and p-AKT/AKT was decreased in the I/R group, but was restored after the pre-treatment with trimetazidine (Fig. 3C).

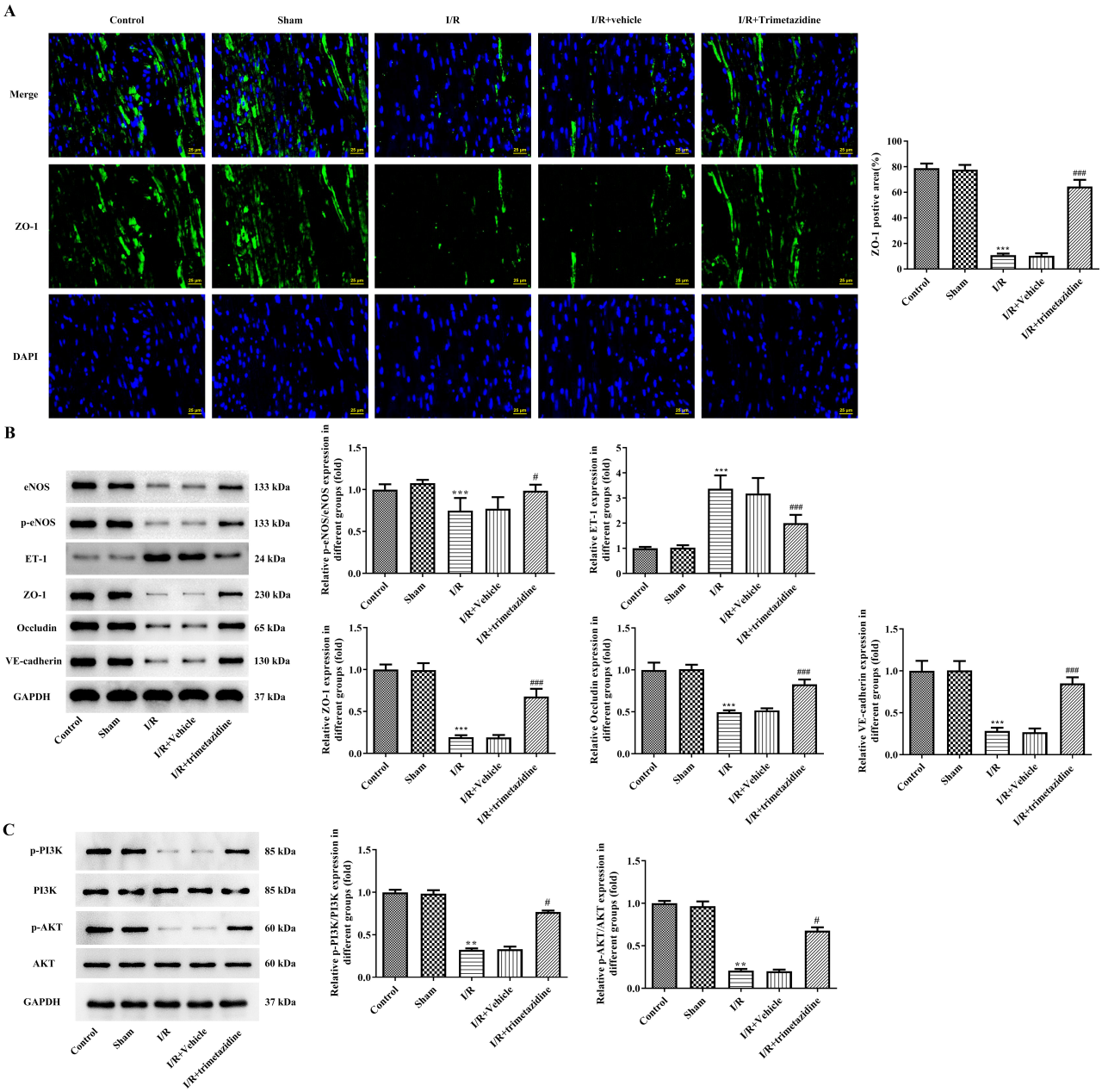

Fig. 3. Trimetazidine improves microvascular reflux, microvascular function and barrier injury during myocardial I/R. (A) IF was used to detect zonula occludens protein 1 (ZO-1) expression (scale bar: 25 μm). (B) Western blot analysis was performed to detect the expressions of endothelial nitric oxide synthase (eNOS), phosphorylated eNOS (p-eNOS), endothelin-1 (ET-1), ZO-1, occludin and vascular endothelial(VE)-cadherin. (C) Western blot analysis was performed to detect the expressions of phosphatidylinositol 3-Kinase (PI3K), phosphorylated PI3K (p-PI3K), Protein Kinase B (AKT), phosphorylated AKT (p-AKT). n = 3, $^{**}p < 0.01$, $^{***}p < 0.001$ vs Sham; $^{\#}p < 0.05$, $^{\#\#\#}p < 0.001$ vs I/R+Vehicle.

3.3 Trimetazidine Regulates AMPK Signaling during Myocardial I/R

The result of WB demonstrated that the expressions of p-AMPK, KLF4 and PPARδ in myocardial tissue of mice were obviously reduced in I/R mice compared with mice in Control and Sham groups. Following the trimetazidine pre-treatment, the expressions of p-AMPK, KLF4 and PPARδ were markedly elevated (Fig. 4).

3.4 Effects of Trimetazidine with Varying Concentrations on the Viability of Primary Mouse Heart Microvascular Endothelial Cells Induced by OGD/R

The extracted mouse heart microvascular endothelial cells were shown in Fig. 5A. To characterize the isolated cell types, we assessed the expression of the endothelial cell marker CD31. The results showed that the extracted cells expressed CD31 (Fig. 5B), indicating that the extracted

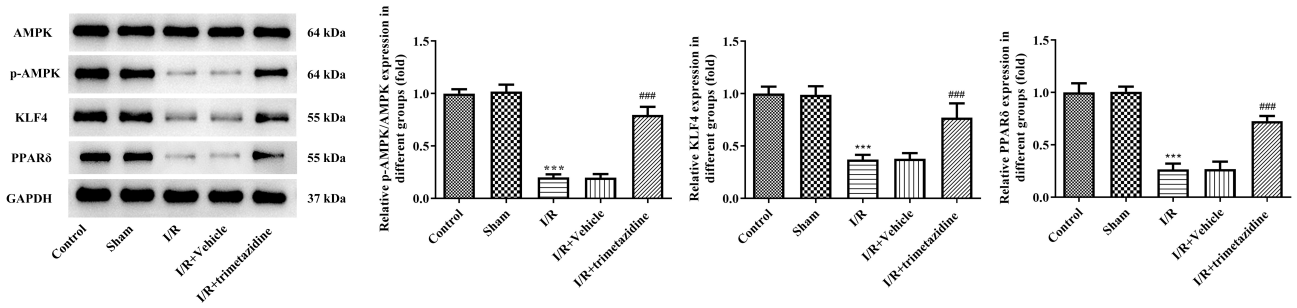

Fig. 4. Trimetazidine regulates the expression of AMPK signaling pathway during myocardial I/R. The expressions of adenosine monophosphate (AMP)-activated protein kinase (AMPK), phosphorylated AMPK (p-AMPK), kruppel-like factor 4 (KLF4) and peroxisome proliferator-activated receptor delta (PPARδ) were detected by western blot. n = 3, ***$p < 0.001$ vs Sham; $^{###}p < 0.001$ vs I/R+Vehicle.

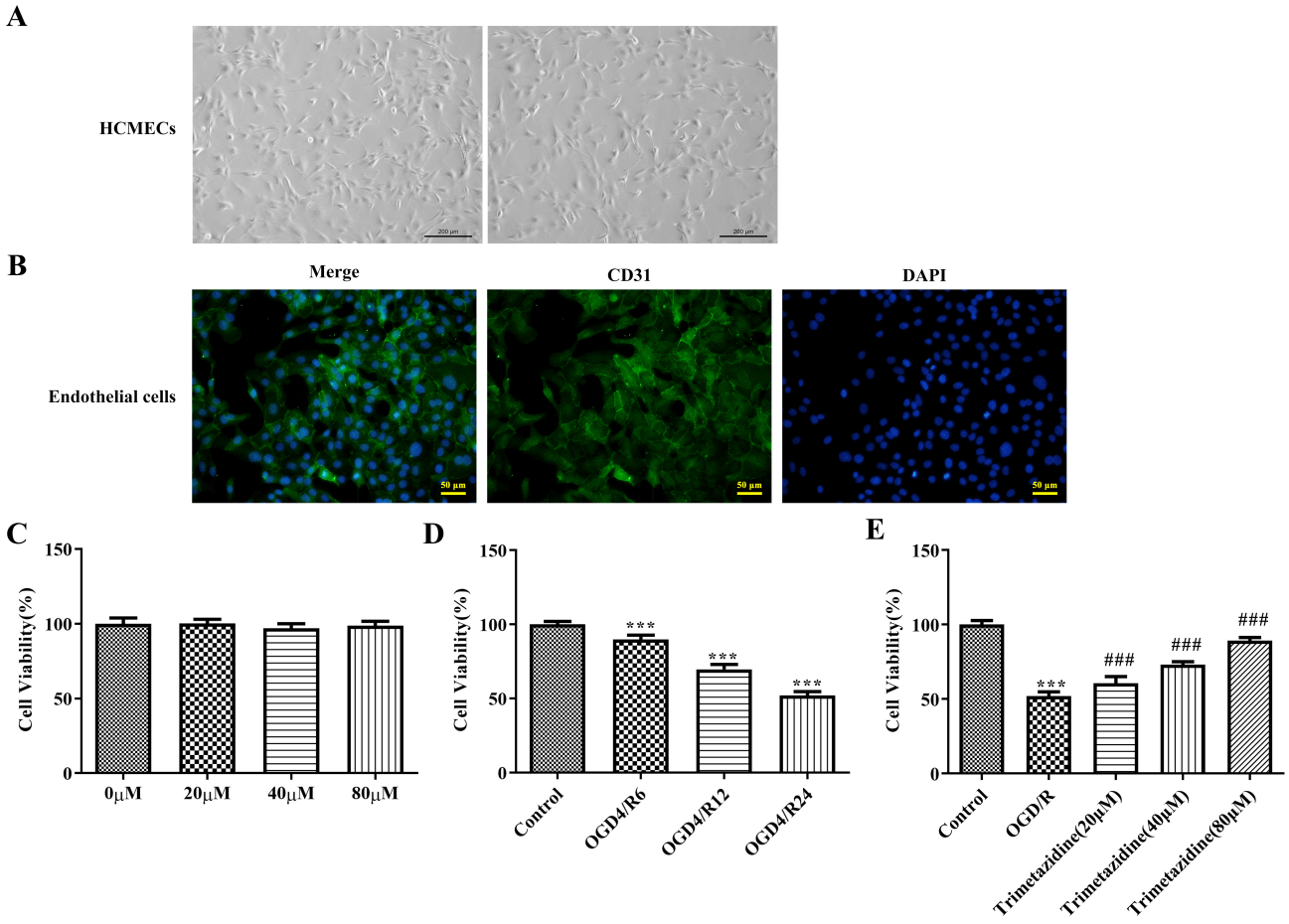

Fig. 5. Effects of trimetazidine with varying concentrations on the viability of primary mouse heart microvascular endothelial cells induced by oxygen-glucose deprivation/reperfusion (OGD/R). (A) Mouse heart microvascular endothelial cells (scale bar: 200 μm). (B) Endothelial cell marker CD31 immunofluorescence identification (scale bar: 50 μm). (C–E) Cell Counting Kit-8 (CCK-8) was used to detect the cell viability. n = 3, ***$p < 0.001$ vs Control; $^{###}p < 0.001$ vs OGD/R.

cells were endothelial cells. Different doses of trimetazidine (20, 40, and 80 μM) were adopted to pre-treat primary mouse heart microvascular endothelial cells, and it was discovered that trimetazidine had no significant effect on cell viability (Fig. 5C). Then CCK-8 was employed to evaluate the impacts of reoxygenation time in OGD/R model on cell viability, and it was found that the cell viability was injured with the extension of reoxygenation time. The reoxygenation time with cell viability in the range of about 50%–60% was selected, that is, OGD4/R24 was used as the hy-

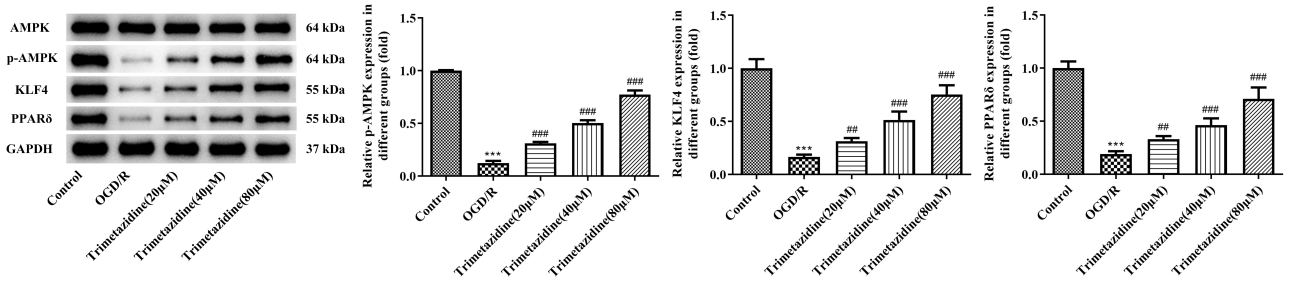

Fig. 6. Effect of trimetazidine with varying concentrations on AMPK signaling pathway in primary mouse heart microvascular endothelial cells induced by OGD/R. Western blot assay was used to detect the expressions of AMPK signaling pathway-related proteins. n = 3, ***$p < 0.001$ vs Control; $^{\#\#}p < 0.01$, $^{\#\#\#}p < 0.001$ vs OGD/R.

poxia reoxygenation condition for further study (Fig. 5D). The cells were grouped into Control, OGD/R, trimetazidine (20 μM), trimetazidine (40 μM) and trimetazidine (80 μM). Results obtained from CCK-8 results presented that the viability of cell in OGD/R group was dramatically reduced by contrast with that in Control group, which was the partially revived by trimetazidine treatment with dose-dependent (Fig. 5E).

3.5 Effect of Trimetazidine with Varying Concentrations on AMPK Signaling Pathway in OGD/R Induced Primary Mouse Heart Microvascular Endothelial Cells

WB was selected as the method of estimation for AMPK signaling pathway-associated proteins. The results indicated that the p-AMPK, KLF4 and PPARδ expressions in OGD/R groups were conspicuously diminished, which were concentration dependently ascended by trimetazidine treatment (Fig. 6). Given the distinctive regulatory impart of trimetazidine at 80 μM concentration on AMPK signaling pathway in cells, 80 μM trimetazidine was adopted for follow-up experiments.

3.6 Trimetazidine Alleviates the Viability and Apoptosis of OGD/R-Induced Primary Mouse Heart Microvascular Endothelial Cells through AMPK Signaling Pathway

Subsequently, we applied trimetazidine together with an AMPK inhibitor compound C to the cells. Results obtained from WB elucidated that the decreased contents of p-AMPK, KLF4 and PPARδ in OGD/R group were elevated by trimetazidine treatment, which were then decreased again following compound C treatment (Fig. 7A). Additionally, cell viability in OGD/R group showed a significant decline, which was then improved by trimetazidine treatment. Relative to the OGD/R+trimetazidine group, compound C administration diminished the cell viability again (Fig. 7B). As Fig. 7C depicted, the induced apoptosis in OGD/R group was suppressed by trimetazidine treatment, while compound C imparted opposite impacts on it, evidenced by increased apoptosis in OGD/R+trimetazidine+Compound C group.

3.7 Trimetazidine Alleviates Functional Impairment of OGD/R-Induced Primary Mouse Heart Microvascular Endothelial Cells through AMPK Signaling Pathway

Results obtained from WB exhibited a reduction in eNOS and p-eNOS contents and an ascending ET-1 expression in OGD/R group, which were then reversed following the pre-treatment of trimetazidine. However, compound C attenuated the effect of trimetazidine (Fig. 8A). Relative to the OGD/R group, trimetazidine pre-treatment led to a notable elevation in NO level, which was subsequently declined again following the administration of compound C (Fig. 8B). The results of WB assay showed that the ratio of p-PI3K/PI3K and p-AKT/AKT was increased after the pre-treatment with trimetazidine compared with the OGD/R group. Also, compound C attenuated the effect of trimetazidine (Fig. 8C). Results obtained from tubule formation presented that the tube number in OGD/R cells was remarkably decreased, which was then increased following trimetazidine pre-treatment. By contrast with the OGD/R+trimetazidine group, compound C administration diminished the tube number again (Fig. 8D). Relative to the OGD/R group, trimetazidine treatment greatly elevated the contents of CD31 and VEGF, which were subsequently reduced after the addition of compound C (Fig. 8E).

3.8 Trimetazidine Alleviates Barrier Damage of OGD/R-Induced Primary Mouse Heart Microvascular Endothelial Cells through AMPK Signaling Pathway

The endothelial cell permeability experiment demonstrated that the fluorescence value in OGD/R group was increased, which was then reduced following the pre-treatment of trimetazidine. However, the addition of compound C led to an increase in fluorescence values compared with the OGD/R+trimetazidine group (Fig. 9A). The expression of VE-cadherin was detected by IF to investigate the integrity of cell membrane and the results illustrated that VE-cadherin fluorescence brightness was dimmed in OGD/R group, indicating that cell membrane integrity was injured. Nevertheless, the damaged cell membrane integrity in OGD/R group was subsequently improved by trimetazidine pretreatment (Fig. 9B). Additionally, it was

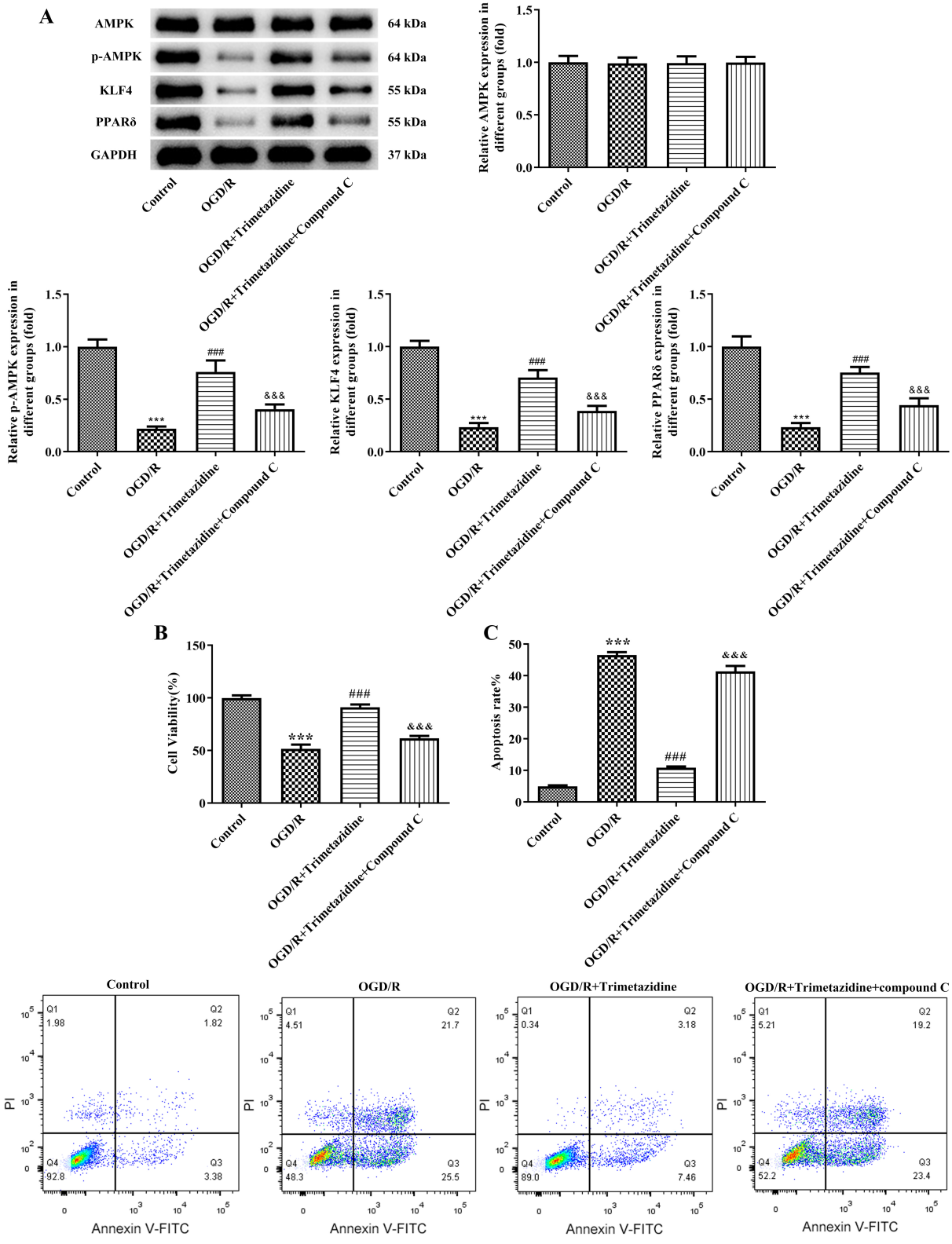

Fig. 7. Trimetazidine alleviates the viability and the apoptosis of OGD/R-induced primary mouse heart microvascular endothelial cells through AMPK signaling pathway. (A) Western blot was used to detect the expressions of AMPK signaling pathway-related proteins. (B) CCK-8 was used to detect cell viability. (C) Flow cytometry was used to detect cell apoptosis. n = 3, $^{***}p < 0.001$ vs Control; $^{\#\#\#}p < 0.001$ vs OGD/R; $^{\&\&\&}p < 0.001$ vs OGD/R+ trimetazidine.

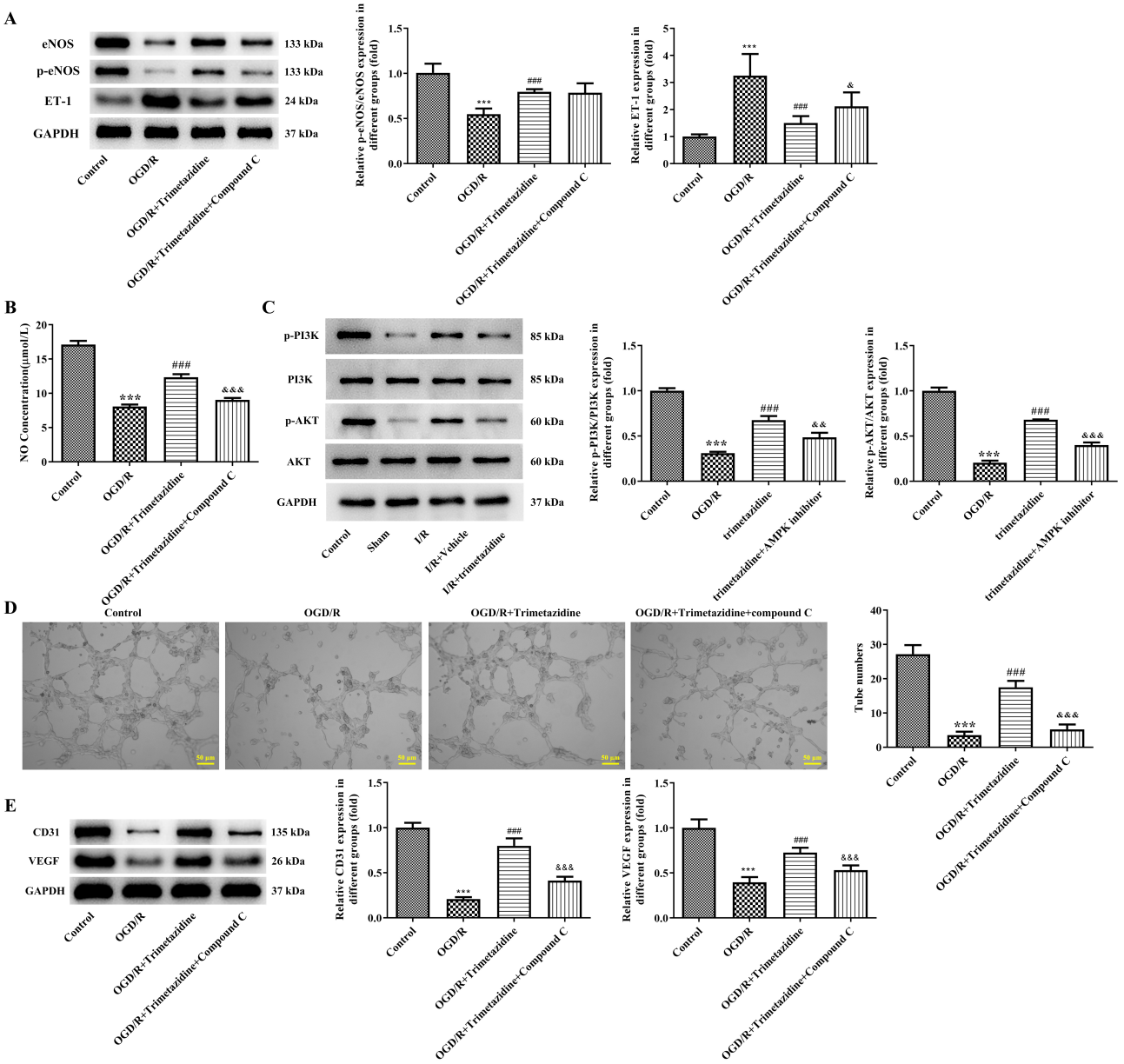

Fig. 8. Trimetazidine alleviates functional impairment of OGD/R-induced primary mouse heart microvascular endothelial cells through AMPK signaling pathway. (A) The expressions of eNOS, p-eNOS and ET-1 were detected by western blot. (B) The NO expression in cell supernatant was detected by the Kit. (C) The expressions of p-PI3K, PI3K, p-AKT, AKT were detected by western blot. (D) The number of tubules was detected by tubule formation assay (scale bar: 50 μm). (E) The expressions of Cd31 and vascular endothelial growth factor (VEGF) were detected by western blot. n = 3, $^{***}p < 0.001$ vs Control; $^{\#\#\#}p < 0.001$ vs OGD/R; $^{\&}p < 0.05$, $^{\&\&}p < 0.01$, $^{\&\&\&}p < 0.001$ vs OGD/R+ trimetazidine.

observed that the declined contents of ZO-1, Occludin and VE-cadherin in the OGD/R group were elevated following trimetazidine pre-treatment (Fig. 9C). The fluorescence intensity of ZO-1 was increased in trimetazidine group compared with the OGD/R group (Fig. 9D). However, compound C reversed the effect of trimetazidine on VE-cadherin, ZO-1 and Occludin expression.

4. Discussion

CMD is the underlying cause of ischemic heart disease. A reduction in coronary flow reserve is related to an increased risk of myocardial infarction size, a decline in left ventricular EF and FS, and impaired left ventricular remodeling [18–20]. The outcomes of percutaneous coronary intervention (PCI) treatment for patients suffering from microvascular dysfunction are not satisfied. However, reperfusion paradoxically contributes to additional tis-

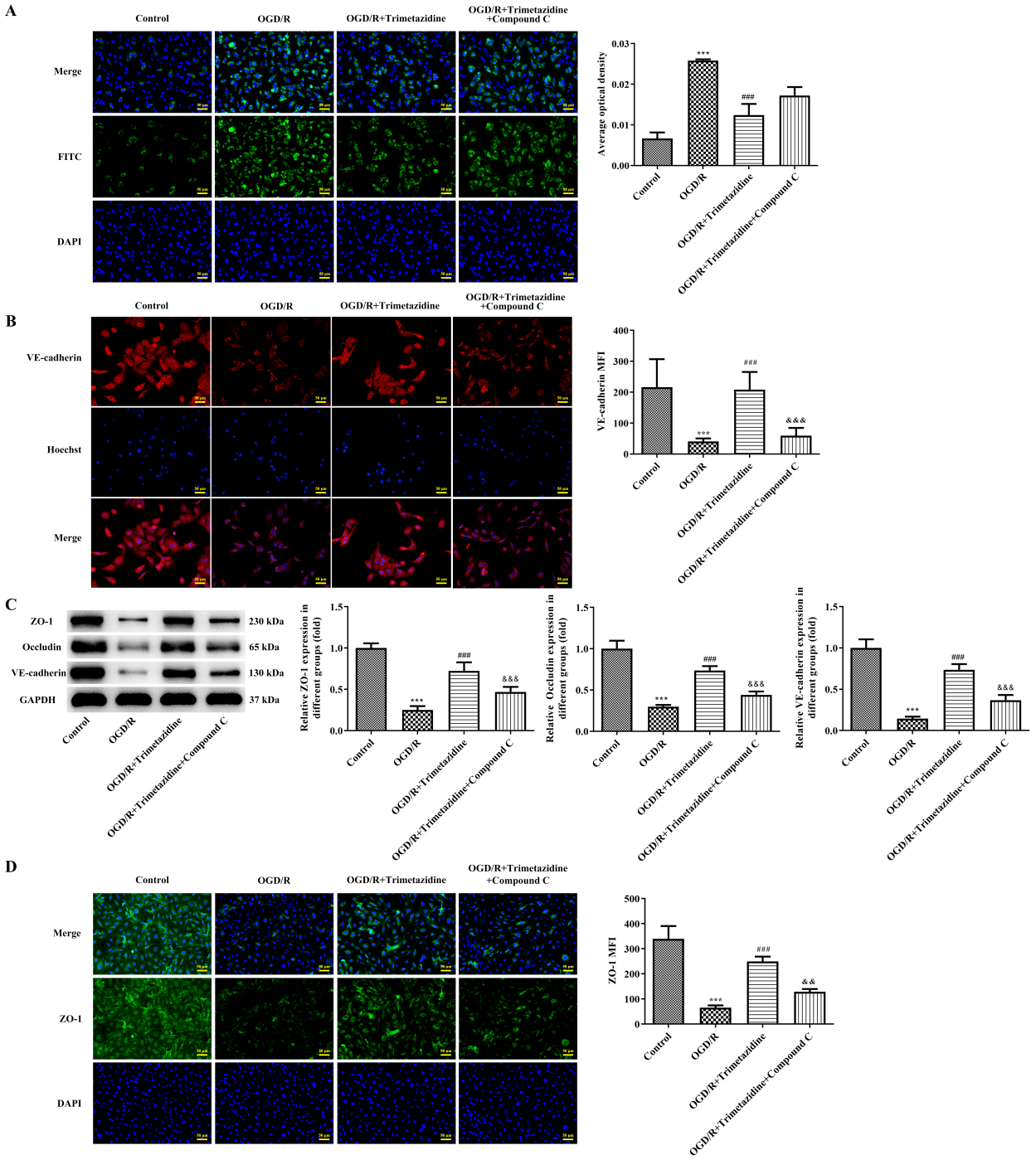

Fig. 9. Trimetazidine alleviates barrier damage of OGD/R-induced primary mouse heart microvascular endothelial cells through AMPK signaling pathway. (A) The endothelial cell permeability experiment was used to detect the cell permeability (scale bar: 50 μm). (B) The expression of VE-cadherin was detected by IF to investigate the integrity of cell membrane (scale bar: 50 μm). (C) Western blot detected the expressions of ZO-1, Occludin and VE-cadherin. (D) IF was used to detect ZO-1 expression (scale bar: 50 μm). n = 3, $^{***}p < 0.001$ vs Control; $^{\#\#\#}p < 0.001$ vs OGD/R; $^{\&\&}p < 0.01$, $^{\&\&\&}p < 0.001$ vs OGD/R+trimetazidine.

sue damage, which results in patients developing muscle damage and heart failure [21]. Therefore, maintaining normal microvascular function after myocardial infarction has emerged as a cruical element in the management of the condition.

CMD is characterized by abnormal structure and function of coronary microvessels with a vessel diameter within 500 μm, contributing to a disparity in blood and oxygen supply to the myocardium [9]. The disruption of coronary microvascular endothelium, platelet adhesion and inflam-

matory response promote the *in-situ* formation of thrombosis and microvascular occlusion, which are the primary causes of CMD [10,11]. Therefore, effective improvement of coronary microvascular endothelial injury is very important to restore coronary microcirculation and enhance myocardial I/R.

The previous study has shown that trimetazidine belongs to a new class of drugs promoting myocardial metabolism, which can help to relax myocardium, suppress myocardial ischemia, and improve the cardiac function of patients [22]. trimetazidine exhibited protective effects on myocardial I/R by inhibiting excessive autophagy [23]. In addition, trimetazidine could improve rat myocardium after I/R injury by effectively alleviating myocardial apoptosis injury, which is of great value for myocardial ischemia and reperfusion treatment [24]. However, it remains unclear whether it can reduce the damage to endothelial cells during myocardial I/R. In our experiment, it was discovered that trimetazidine can alleviate myocardial pathological injury and cardiac dysfunction, improve microvascular reflux phenomenon and microvascular function and alleviate barrier injury during myocardial I/R. In cell experiments, trimetazidine could promote the viability and inhibit the apoptosis of OGD/R-induced primary mouse heart microvascular endothelial cells. Moreover, trimetazidine could alleviate the damage to the function and the barrier of OGD/R-induced primary mouse heart microvascular endothelial cells. It has been shown that trimetazidine could reduce endothelial dysfunction in ischemic heart disease patients [25]. Additionally, trimetazidine was evidenced to alleviate and prevent endothelial dysfunction caused by PCI in unstable angina pectoris patients [26]. The above-mentioned findings are consistent with our experimental investigation. Our outcomes revealed that trimetazidine could improve myocardial I/R injury-induced endothelial cell disfunction, thereby improving CMD.

Studies have shown that trimetazidine can stimulate the expression of AMPK signal in cardiomyocytes [22,27], and the activation of AMPK can improve myocardial I/R injury [28] and promote eNOS expression in myocardial I/R tissues [29]. Meanwhile, it has been reported that AMPK can mitigate endothelial cell dysfunction resulting from elevated glucose levels by activating downstream PPARδ [30]. Besides, AMPK was involved in alleviating endothelial cell aging and dysfunction induced by high sugar levels via KLF4 signal [31]. The above-mentioned findings indicated that the activation of AMPK signal was involved in endothelial cell dysfunction by regulating the downstream signal. In our experiments, the results exhibited that trimetazidine activated the AMPK signaling in myocardial I/R mice and OGD/R-induced primary mouse microvascular endothelial cells. Further administration of AMPK signaling pathway inhibitor compound C attenuated the protective effects of trimetazidine on primary mouse microvascular endothelial cells induced by OGD/R.

Myocardial ischemia is caused by epicardial coronary artery stenosis or atherosclerotic disease affecting microcirculation. Trimetazidine promotes glucose oxidation which optimizes cellular energy processes in ischemic conditions. A study have demonstrated that trimetazidine treatment prior to elective percutaneous coronary intervention (PCI) reduced microvascular dysfunction by lowering post-procedural index of microcirculatory resistance (IMR) values [32]. There has been a lack of research into how trimetazidine enhances vascular ring function. This study is the first to examine the mechanisms by which trimetazidine alleviates microvascular dysfunction resulting from myocardial infarction and ischemia-reperfusion. The findings reveal that trimetazidine enhances the function and mitigates barrier damage in mouse heart microvascular endothelial cells by modulating the PI3K/AKT/eNOS/NO signaling pathway. Additionally, prior research has indicated that trimetazidine can stimulate AMPK signaling in cardiomyocytes [22,27], which helps to alleviate myocardial ischemia-reperfusion injury [28]. In this study, we noted the activation of AMPK signaling in heart microvascular endothelial cells, and the protective effects of trimetazidine on these cells were significantly diminished when AMPK signaling was inhibited. This suggests that trimetazidine activates the AMPK signaling pathway not only in cardiomyocytes during ischemia-reperfusion but also in heart microvascular endothelial cells. Furthermore, we discovered that the AMPK signaling pathway inhibitor compound C notably reduced the protective effects of trimetazidine on the function and barrier integrity of heart microvascular endothelial cells and inhibited the activation of the PI3K/AKT/eNOS/NO signaling pathway. This indicated that trimetazidine's regulation of the PI3K/AKT signaling pathway in mouse heart microvascular endothelial cells was mediated through the AMPK signaling pathway.

5. Conclusion

Trimetazidine could improve CMD induced by myocardial infarction by activating AMPK signal. Our study offers a theoretical basis for trimetazidine in the clinical treatment of CMD caused by myocardial infarction.

Availability of Data and Materials

Original data of this study are available from the corresponding author on request.

Author Contributions

XQ and YY designed the experiment research. XQ, PY and LJ performed the experiments. XQ performed formal analyses and wrote the original manuscript. PY and YY contributed to the conception and design of the work. All authors have revised the manuscript and approved the final manuscript. All authors have participated sufficiently in the work and agreed to be accountable for all aspects of the work.

Ethics Approval and Consent to Participate

All animal experiments were approved by the ethical committee of Zhaofenghua Biotechnology [IACUC-20221009-03].

Acknowledgment

Not applicable.

Funding

This research received no external funding.

Conflict of Interest

The authors declare no conflict of interest.

References

[1] Abdu FA, Mohammed AQ, Liu L, Xu Y, Che W. Myocardial Infarction with Nonobstructive Coronary Arteries (MINOCA): A Review of the Current Position. Cardiology. 2020; 145: 543–552. https://doi.org/10.1159/000509100.

[2] Wu JW, Hu H, Hua JS, Ma LK. ATPase inhibitory factor 1 protects the heart from acute myocardial ischemia/reperfusion injury through activating AMPK signaling pathway. International Journal of Biological Sciences. 2022; 18: 731–741. https://doi.org/10.7150/ijbs.64956.

[3] Zhang G, Wang X, Li C, Li Q, An YA, Luo X, *et al*. Integrated Stress Response Couples Mitochondrial Protein Translation With Oxidative Stress Control. Circulation. 2021; 144: 1500–1515. https://doi.org/10.1161/CIRCULATIONAHA.120.053125.

[4] Xu C, Wang J, Fan Z, Zhang S, Qiao R, Liu Y, *et al*. Cardioprotective effects of melatonin against myocardial ischaemia/reperfusion injury: Activation of AMPK/Nrf2 pathway. Journal of Cellular and Molecular Medicine. 2021; 25: 6455–6459. (online ahead of print) https://doi.org/10.1111/jcmm.16691.

[5] Kang MG, Koo BK, Tantry US, Kim K, Ahn JH, Park HW, *et al*. Association Between Thrombogenicity Indices and Coronary Microvascular Dysfunction in Patients With Acute Myocardial Infarction. JACC. Basic to Translational Science. 2021; 6: 749–761. https://doi.org/10.1016/j.jacbts.2021.08.007.

[6] Bularga A, Taggart C, Mendusic F, Kimenai DM, Wereski R, Lowry MTH, *et al*. Assessment of Oxygen Supply-Demand Imbalance and Outcomes Among Patients With Type 2 Myocardial Infarction: A Secondary Analysis of the High-STEACS Cluster Randomized Clinical Trial. JAMA Network Open. 2022; 5: e2220162. https://doi.org/10.1001/jamanetworkopen.2022.20162.

[7] Heusch G, Skyschally A, Kleinbongard P. Coronary microembolization and microvascular dysfunction. International Journal of Cardiology. 2018; 258: 17–23. https://doi.org/10.1016/j.ijcard.2018.02.010.

[8] Kloka JA, Friedrichson B, Wülfroth P, Henning R, Zacharowski K. Microvascular Leakage as Therapeutic Target for Ischemia and Reperfusion Injury. Cells. 2023; 12: 1345. https://doi.org/10.3390/cells12101345.

[9] Camici PG, d'Amati G, Rimoldi O. Coronary microvascular dysfunction: mechanisms and functional assessment. Nature Reviews. Cardiology. 2015; 12: 48–62. https://doi.org/10.1038/nrcardio.2014.160.

[10] Taqueti VR, Di Carli MF. Coronary Microvascular Disease Pathogenic Mechanisms and Therapeutic Options: JACC State-of-the-Art Review. Journal of the American College of Cardiology. 2018; 72: 2625–2641. https://doi.org/10.1016/j.jacc.2018.09.042.

[11] Jackson SP, Darbousset R, Schoenwaelder SM. Thromboinflammation: challenges of therapeutically targeting coagulation and other host defense mechanisms. Blood. 2019; 133: 906–918. https://doi.org/10.1182/blood-2018-11-882993.

[12] Heggermont WA, Papageorgiou AP, Heymans S, van Bilsen M. Metabolic support for the heart: complementary therapy for heart failure? European Journal of Heart Failure. 2016; 18: 1420–1429. https://doi.org/10.1002/ejhf.678.

[13] Chen X, Lin S, Dai S, Han J, Shan P, Wang W, *et al*. Trimetazidine affects pyroptosis by targeting GSDMD in myocardial ischemia/reperfusion injury. Inflammation Research. 2022; 71: 227–241. https://doi.org/10.1007/s00011-021-01530-6.

[14] Qian G, A X, Jiang X, Jiang Z, Li T, Dong W, *et al*. Early Trimetazidine Therapy in Patients Undergoing Primary Percutaneous Coronary Intervention for ST Segment Elevation Myocardial Infarction Reduces Myocardial Infarction Size. Cardiovascular Drugs and Therapy. 2023; 37: 497–506. https://doi.org/10.1007/s10557-021-07259-y.

[15] Chen X, Xia X, Dong T, Lin Z, Du L, Zhou H. Trimetazidine Reduces Cardiac Fibrosis in Rats by Inhibiting NOX2-Mediated Endothelial-to-Mesenchymal Transition. Drug Design, Development and Therapy. 2022; 16: 2517–2527. https://doi.org/10.2147/DDDT.S360283.

[16] Sonin D, Papayan G, Istomina M, Anufriev I, Pochkaeva E, Minasian S, *et al*. Advanced technique of myocardial no-reflow quantification using indocyanine green. Biomedical Optics Express. 2024; 15: 818–833. https://doi.org/10.1364/BOE.511912.

[17] Li Q, Guo Z, Wu C, Tu Y, Wu Y, Xie E, *et al*. Ischemia preconditioning alleviates ischemia/reperfusion injury-induced coronary no-reflow and contraction of microvascular pericytes in rats. Microvascular Research. 2022; 142: 104349. https://doi.org/10.1016/j.mvr.2022.104349.

[18] Chang X, Lochner A, Wang HH, Wang S, Zhu H, Ren J, *et al*. Coronary microvascular injury in myocardial infarction: perception and knowledge for mitochondrial quality control. Theranostics. 2021; 11: 6766–6785.

[19] Dean J, Cruz SD, Mehta PK, Merz CNB. Coronary microvascular dysfunction: sex-specific risk, diagnosis, and therapy. Nature Reviews. Cardiology. 2015; 12: 406–414. https://doi.org/10.1038/nrcardio.2015.72.

[20] Fordyce CB, Gersh BJ, Stone GW, Granger CB. Novel therapeutics in myocardial infarction: targeting microvascular dysfunction and reperfusion injury. Trends in Pharmacological Sciences. 2015; 36: 605–616. https://doi.org/10.1016/j.tips.2015.06.004.

[21] Kelly DJ, Gershlick T, Witzenbichler B, Guagliumi G, Fahy M, Dangas G, *et al*. Incidence and predictors of heart failure following percutaneous coronary intervention in ST-segment elevation myocardial infarction: the HORIZONS-AMI trial. American Heart Journal. 2011; 162: 663–670. https://doi.org/10.1016/j.ahj.2011.08.002.

[22] Shu H, Peng Y, Hang W, Zhou N, Wang DW. Trimetazidine in Heart Failure. Frontiers in Pharmacology. 2021; 11: 569132. https://doi.org/10.3389/fphar.2020.569132.

[23] Wu S, Chang G, Gao L, Jiang D, Wang L, Li G, *et al*. Trimetazidine protects against myocardial ischemia/reperfusion injury by inhibiting excessive autophagy. Journal of Molecular Medicine (Berlin, Germany). 2018; 96: 791–806. https://doi.org/10.1007/s00109-018-1664-3.

[24] He C, Cao S, Tong Z, Wang W, Zhang Y, Guo C. Trimetazidine ameliorates myocardial ischemia-reperfusion injury. Pakistan Journal of Pharmaceutical Sciences. 2018; 31: 1691–1696.

[25] Rehberger-Likozar A, Šebeštjen M. Influence of trimetazidine and ranolazine on endothelial function in patients with ischemic

heart disease. Coronary Artery Disease. 2015; 26: 651–656. https://doi.org/10.1097/MCA.0000000000000272.

[26] Shao S, Shi Z, Tse G, Wang X, Ni Y, Liu H, *et al*. Effects of Trimetazidine Pretreatment on Endothelial Dysfunction and Myocardial Injury in Unstable Angina Patients Undergoing Percutaneous Coronary Intervention. Cardiology Research and Practice. 2019; 2019: 4230948. https://doi.org/10.1155/2019/4230948.

[27] Shu H, Hang W, Peng Y, Nie J, Wu L, Zhang W, *et al*. Trimetazidine Attenuates Heart Failure by Improving Myocardial Metabolism via AMPK. Frontiers in Pharmacology. 2021; 12: 707399. https://doi.org/10.3389/fphar.2021.707399.

[28] Tian L, Cao W, Yue R, Yuan Y, Guo X, Qin D, *et al*. Pretreatment with Tilianin improves mitochondrial energy metabolism and oxidative stress in rats with myocardial ischemia/reperfusion injury via AMPK/SIRT1/PGC-1 alpha signaling pathway. Journal of Pharmacological Sciences. 2019; 139: 352–360. https://doi.org/10.1016/j.jphs.2019.02.008.

[29] Kim AS, Miller EJ, Wright TM, Li J, Qi D, Atsina K, *et al*. A small molecule AMPK activator protects the heart against ischemia-reperfusion injury. Journal of Molecular and Cellular Cardiology. 2011; 51: 24–32. https://doi.org/10.1016/j.yjmcc.2011.03.003.

[30] Liu F, Fang S, Liu X, Li J, Wang X, Cui J, *et al*. Omentin-1 protects against high glucose-induced endothelial dysfunction via the AMPK/PPARδ signaling pathway. Biochemical Pharmacology. 2020; 174: 113830. https://doi.org/10.1016/j.bcp.2020.113830.

[31] Wang G, Han B, Zhang R, Liu Q, Wang X, Huang X, *et al*. C1q/TNF-Related Protein 9 Attenuates Atherosclerosis by Inhibiting Hyperglycemia-Induced Endothelial Cell Senescence Through the AMPKα/KLF4 Signaling Pathway. Frontiers in Pharmacology. 2021; 12: 758792. https://doi.org/10.3389/fphar.2021.758792.

[32] Ilic I, Timcic S, Milosevic M, Boskovic S, Odanovic N, Furtula M, *et al*. The imPAct of Trimetazidine on MicrOcirculation after Stenting for stable coronary artery disease (PATMOS study). Frontiers in Cardiovascular Medicine. 2023; 10: 1112198. https://doi.org/10.3389/fcvm.2023.1112198.